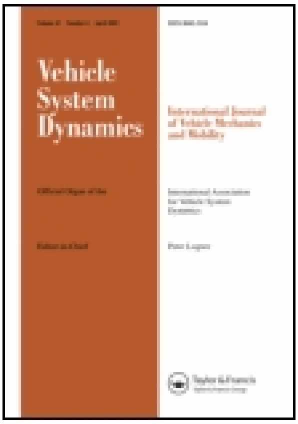

Vehicle System Dynamics
Publication details, including instructions for authors and subscription information:
http://www.tandfonline.com/loi/nvsd20

The dynamic study of locomotives under saturated adhesion

Yao Yuan [a], Zhang Hong-jun [a], Li Ye-ming [b] & Luo Shi-hui [a]

[a] Traction Power State Key Laboratory, Southwest JiaoTong University, Chengdu, People's Republic of China

[b] Locomotive & Car Research Institute, China Academy of Railway Sciences, Beijing, China

Available online: 07 Jul 2011

To cite this article: Yao Yuan, Zhang Hong-jun, Li Ye-ming & Luo Shi-hui (2011): The dynamic study of locomotives under saturated adhesion, Vehicle System Dynamics, 49:8, 1321-1338

To link to this article: http://dx.doi.org/10.1080/00423111003668195

Vehicle System Dynamics
Vol. 49, No. 8, August 2011, 1321–1338

The dynamic study of locomotives under saturated adhesion

Yao Yuan[a]*, Zhang Hong-jun[a], Li Ye-ming[b] and Luo Shi-hui[a]

[a]*Traction Power State Key Laboratory, Southwest JiaoTong University, Chengdu, People's Republic of China;* [b]*Locomotive & Car Research Institute, China Academy of Railway Sciences, Beijing, China*

(*Received 20 August 2009; final version received 31 January 2010*)

In order to study the dynamic behaviours of locomotives under saturated adhesion, the stability and characteristics of stick–slip vibration are analysed using the concepts of mean and dynamic slip rates. The longitudinal vibration phenomenon of the wheelset when stick–slip occurs is put forward and its formation mechanism is made clear innovatively. The stick–slip vibration is a dynamic process between the stick and the slip states. The decreasing of mean and dynamic slip rates is conducive to its stability, which depends on the W/R adhesion damping. The torsion vibration of the driving system and the longitudinal vibration of the wheelset are coupled through the longitudinal tangential force when the wheelset alternates between the stick and the slip states. The longitudinal oscillation frequencies of the wheelset are integral multiples of the natural frequency of torsion vibration of the driving system. A train dynamic model integrated with an electromechanical and a control system is established to simulate the stick–slip vibration phenomenon under saturated adhesion to verify the theoretical analysis. The results show that increases of the longitudinal axle guidance stiffness and the motor suspension stiffness are beneficial to the stick–slip vibration stability and the locomotive's traction ability. The optimised matching of the longitudinal axle guidance stiffness and the motor suspension stiffness are helpful to avoid longitudinal resonance when the stick–slip vibration occurs.

Keywords: driving dynamics; stick–slip vibration; longitudinal vibration; locomotive; saturated adhesion; parameter matching

1. Introduction

With high power railway locomotives being put into use, the increase in locomotive traction power is restricted by the effective utilisation of the wheel/rail adhesion. The saturation and negative slope characteristics of adhesion cause locomotives some complex dynamic problems. Important theoretical and engineering applications can be made if the locomotive's dynamic behaviours under saturated adhesion are understood and the bogie structure parameters can be matched reasonably to improve the traction force and reduce the dynamic force.

The wheel/rail adhesion cannot be maintained at the peak of W/R tangential force coefficient and get into slip state easily because of negative slope characteristic of adhesion cures when the large relative sliding occurs. Researchers found these complex problems in driving processes and started to investigate locomotive driving dynamics long ago. Hirotsu *et al.* [1]

*Corresponding author. Email: yyuan8848@163.com

ISSN 0042-3114 print/ISSN 1744-5159 online

DOI: 10.1080/00423111003668195
http://www.informaworld.com

tested the self-excited vibration with experiments and indicated that the increases in stiffness and damping of locomotive structure are helpful to restrain the vibration. Wu [2] proposed the concept of stick–slip vibration and analysed the vibration stability of the driving system on bogie-mounted locomotives with simulation. Muller and Kogel [3] analysed the wheelset rolling-slip vibrations under inconsistent adhesion on the left and right wheels. Sun [4] established a mechanical–electrical driving dynamic model to study the effects on stick–slip vibration of locomotives with different characteristics and control strategies of electric driving system. Sun also proposed an integrative design principle of ‘Traction system-Bogie-Control System’ about high adhesion locomotives. Some literature [5,6] reported the experimental investigation of transient traction characteristics in rolling–sliding wheel/rail contacts, and Polach [7,8] presented a fast wheel–rail force calculation computer code, which included the negative slope characteristic and the effects on different rail adhesion conditions. The mechanism of stick–slip vibration was studied for the locomotives design, but they did not find the coupling phenomenon between the stick–slip vibration and the wheelset longitudinal vibration.

In this paper, we use a simplified dynamic model with a single wheelset driving system to illuminate the mechanism and dynamic characteristics of stick–slip vibration based on the concepts of mean and dynamic slip rates. The longitudinal vibration phenomenon of the wheelset, while stick–slip vibration occurs, is presented and its formation mechanism is made clear innovatively. Then, a train’s dynamic model integrated with an electromechanical and a control system is established to verify the theoretical analysis by simulating the phenomenon of stick–slip vibration under saturated adhesion using the software SIMPACK. Finally, we propose the principles of matching the parameter of the high adhesion of locomotives based on the stick–slip vibration theory.

2. Simplified model for theory analysis

2.1. *Single wheel driving system model*

The simplified locomotive driving system is shown in Figure 1. The model has four degrees of freedom and three objects, including a rotor, a wheel and a vehicle. J_m is the rotational inertia of the wheel, m_w and m_b the wheel mass and the vehicle mass, respectively, k_d and c_d the torsional stiffness and damping, respectively, k_x and c_x the longitudinal axle guidance stiffness and damping, respectively, M_m the motor torque, F the vertical load of the wheel, F_0 the traction load.

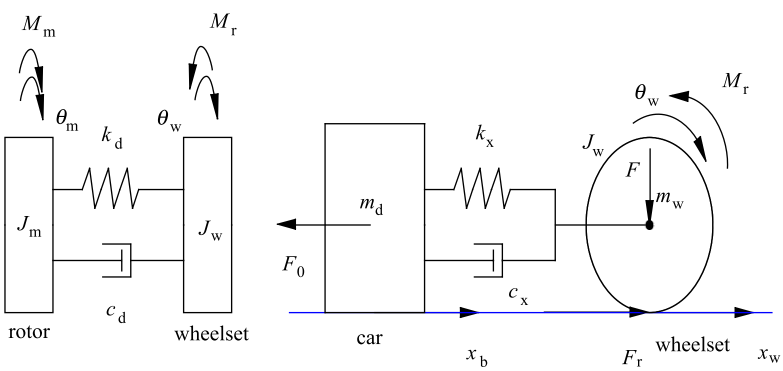

Figure 1. Simplified model on drive system of locomotive.

θ is the relative displacement between the rotor and the wheel and x the relative displacement between the wheel and the vehicle. Assuming the traction torque and the locomotive traction force are constants, the differential equations of the model can be established as follows [9]:

$$\begin{pmatrix} J_w & 0 \\ 0 & m_w \end{pmatrix} \begin{pmatrix} \ddot{\theta} \\ \ddot{x} \end{pmatrix} + \begin{pmatrix} c'_d & 0 \\ 0 & c'_d \end{pmatrix} \begin{pmatrix} \dot{\theta} \\ \dot{x} \end{pmatrix} + \begin{pmatrix} k'_d & 0 \\ 0 & k'_d \end{pmatrix} \begin{pmatrix} \theta \\ x \end{pmatrix} = \begin{pmatrix} -M_r & +M_{r0} \\ F_r & -F_{r0} \end{pmatrix}, \tag{1}$$

where

$$c'_d = c_d\left(1 + \frac{J_w}{J_m}\right), \quad K'_d = k_d\left(1 + \frac{J_w}{J_m}\right), \quad c'_x = c_x\left(1 + \frac{M_w}{M_b}\right), \quad k'_x = k_x\left(1 + \frac{M_w}{M_b}\right).$$

M_r the instantaneous torque, and F_r, the instantaneous force, act on the wheel from the rail. Equation (1) reduces the degrees of freedom of this dynamic system, and defines the mean slip rate easily. The equivalent damping can be defined as follows:

$$F_c(\dot{\theta}, \dot{x}) = \begin{pmatrix} c'_d & 0 \\ 0 & c'_x \end{pmatrix} \begin{pmatrix} \dot{\theta} \\ \dot{x} \end{pmatrix} - \begin{pmatrix} -M_r & +M_{r0} \\ F_r & -F_{r0} \end{pmatrix}. \tag{2}$$

By equating F_c to zero and calculating the eigenvalues of Equation (1), we can obtain natural frequencies of the dynamic system of 38.2 and 12 Hz.

2.2. *Slip rate*

It is well known that the rigid wheel slide occurs, rather than elastic creep during the driving or braking of a locomotive. In order to express the slippage in a more physical sense, we define slip rate for the locomotive driving dynamics as follows:

$$s = \frac{\nu - \omega r}{\nu} = 1 - \frac{(\omega_0 + \dot{\theta})r}{\nu_0 + \dot{x}}, \tag{3}$$

where ν is the instantaneous speed of the wheelset, ν_0 the mean speed, ω the instantaneous angular velocity, ω the mean angular velocity and r the radius of the wheel. When the macroscopic slip of the wheel occurs, the slip rate is a large but limited value compared with the conventional definition of creepage. Under the driving conditions, s is a negative value and we use its absolute value by convenience.

There are few differences between Equation (3) and expressions defined by Carter and UIC [10] only under large slippage of the wheel.

As a dynamical variable, s can be written as follows:

$$s = s_0 + \mathrm{d}s, \tag{4}$$

where s_0 is the mean slip rate and ds the dynamic slip rate. s_0 depends on the traction load of the locomotive and the adhesion condition on the rail, and it is a larger value during slippage. The magnitude of ds is related to the vibrant energy and the elastic connection of the mechanical structures.

If $\dot{x} = 0, \dot{\theta} = 0$, then

$$s_0 = 1 - \frac{\omega_0 r}{v_0}. \tag{5}$$

2.3. *Simplified W/R adhesion curves*

The W/R tangential force coefficient is inversely related to the slip after the peak of adhesion. This is because of the effects of the wheel–rail friction heat and the rail surface roughness [11]. The simplified W/R adhesion curve (Figure 2) can be indicated by a sectional linear function like Equation (6):

$$\mu = \begin{cases} \mu_m s/s_c & 0 \le s < s_c \\ \mu_m + k_\mu (s - s_c) & s_c \le s \end{cases}, \tag{6}$$

where μ_m is the maximum tangential force coefficient, s_c the critical slip rate and k_μ the negative slope on sliding. In the simplified model, we do not take the dispersion of adhesion into account. The adhesion state under positive slope is defined as stick and the negative is defined as slip.

2.4. *The nonlinear damping force*

The instantaneous tangential force and the moment on the wheel have the following relations:

$$F_r = \mu W_0, \quad M_r = F_r r, \tag{7}$$

where F_r consists of the static traction force F_{r0} and the dynamic traction force F_r', M_r consists of the static moment M_{r0} and the dynamic moment M_r' and W_0 is the axle load. Equation (6) can be written as follows:

$$F_r = \begin{cases} W_0 \mu_m s/s_c & 0 \le s < s_c \\ W_0 \mu_m + W_0 k_\mu (s - s_c) & s_c \le s \end{cases}, \tag{8}$$

When $s = s_0$, we can get F_{r0}, M_r and M_{r0}. When s and s_0 are located in the OA and AB section, respectively, in Figure 2, there are four kinds of combinations and four expressions of the equivalent damping force which correspond.

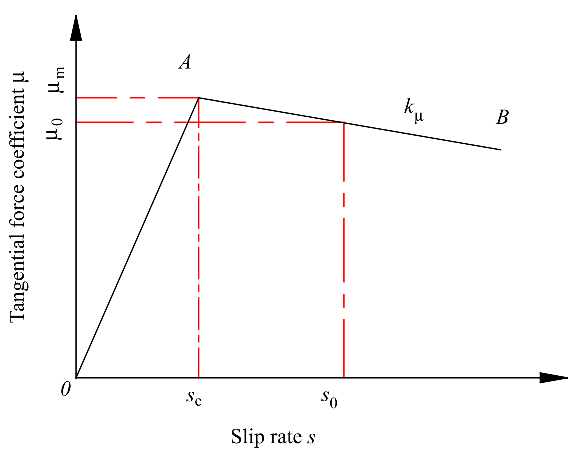

Figure 2. Simplified curve of tangential force coefficient.

3. The stick–slip vibration theory

3.1. *Stick–slip vibration stability*

In the dynamic system, the slip rate is equal to the sum of the mean slip rate and the dynamic slip rate. The mean slip rate depends on the traction working condition and the W/R adhesion state. In Figure 3, the symbol ‘a’ represents stick state, ‘b’ the stick–slip state and ‘c’ the slip state. Ignoring the structure damping, the vibrations on stick state are stable because the positive damping of W/R adhesion dissipates energy and vice versa.

In Figure 4, s_0 is fixed with three different constants, respectively. For Conditions (b) and (c), as the system energy increases, the amplitude of ds will increase until the part of s locates in positive slope of adhesion curves. In other words, when the system is in stick–slip vibration state, the process of increase and consumption of system energy are in balance, and the vibration exists in the limit cycle. Under Condition (c), the value of s_0 is greater than that of Condition (b), and a larger input energy makes it easier to change the wheelset from slippage to stick–slip.

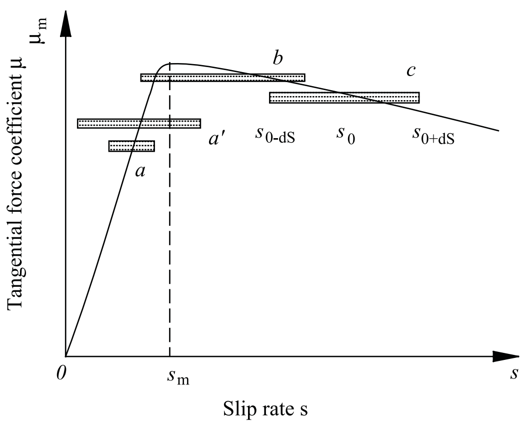

Figure 3. The different states of adhesion.

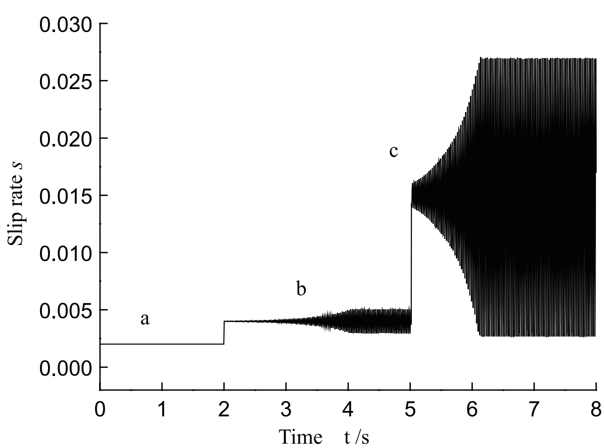

Figure 4. The self-excited vibration of slip rate.

For the practical locomotive in service, s_0 cannot be a constant and ds cannot increase infinitely. In Figure 3, when relating a' with a, because the structure stiffness and damping of the driving system are smaller and the vibration scope of s is wider comparatively, stick state changes into stick–slip vibration state more easily. This increases the system's vibration energy and reaches slip state more quickly. Likewise, when the running state of the wheelset changes from slip into stick, the wide vibration scope of s will extend the time required for re-adhesion.

Many factors influence the re-adhesion of the locomotive, such as rail surface condition, locomotive structural parameters, electric driving system and the mechanical characteristics of the motor. Among these factors, decreasing of the mean slip and the dynamic slip rates are the two most essential approaches to increase the locomotive's re-adhesion ability.

3.2. *The wheelset longitudinal vibration*

Ignoring the effect of damping from the locomotive driving system and the force from inertia, if the slip rate is located in the OA section in Figure 5 and the motor torque is a constant, the positive damping will make the system energy to decrease, and the angular acceleration of the wheelset will be negative. But if the slip rate is located in the AB section, the angular acceleration will be positive. When the tangential force coefficient is greater than the value of μ_0 during the periodic vibration process, which corresponds to the shaded area in Figure 5, the wheelset longitudinal vibration acceleration is positive, and vice versa. During the stick–slip process of the wheelset, the minimum and maximum slip rate are located on both sides of s_0, respectively. The minimum value is less than s_c, as shown in Figure 5. Points 1 and 2 are the corresponding tangential force coefficients of s_1 and s_2, respectively. When the slip rate changes in the cycle of 's_1–s_2–s_1', the wheelset angular velocity will be in the cycle 'decrease–increase–decrease'. However, the change process of the wheelset's longitudinal vibration velocity is 'decrease–increase–decrease–increase–decrease'. The wave frequency of the wheelset's longitudinal vibration acceleration is double the frequency of the wheelset's rotary vibration acceleration. The time domain curves of rotary and the longitudinal vibration accelerations of the wheelset are shown in Figure 6.

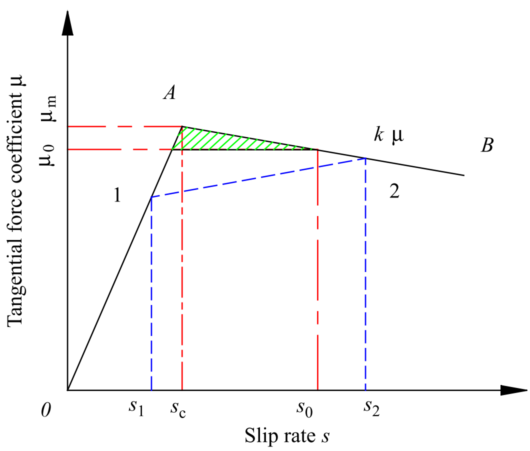

Figure 5. Graphic analysis of stick–slip vibration mechanism.

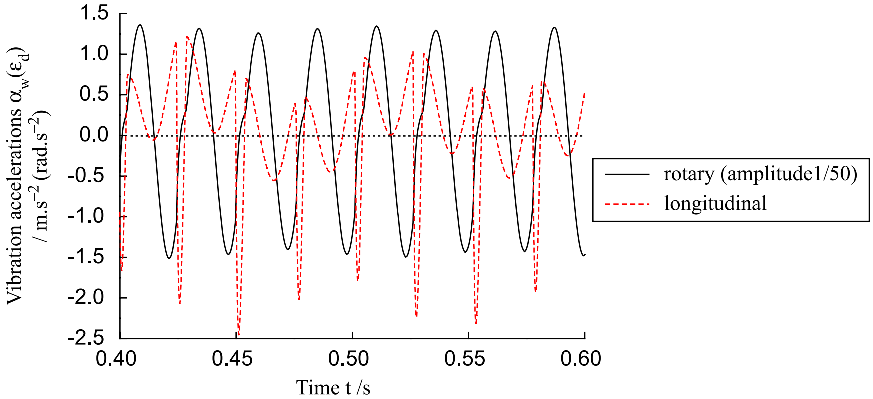

Figure 6. Rotary and longitudinal vibration accelerations of wheelset.

Figure 7 is a frequency spectrum of the wheelset rotary vibration angular acceleration, the frequency of 38 Hz is the main frequency of the rotary vibration and the natural frequency of the driving system. Figure 8 shows the wheelset's longitudinal vibration acceleration frequency spectrum, where 12 Hz is the natural frequency of the longitudinal vibration. These are the same as the eigenvalue calculations from Equation (1). The longitudinal vibration frequencies of the wheelset contain the natural frequency and its integral multiples of the torsional vibration of the driving system. The vibration energy reaches its maximum at twice the natural frequency [12].

If the matching of the torsional stiffness of the driving system and the longitudinal axle guidance stiffness of the locomotive is unreasonable, and the wheelset longitudinal vibration frequency is an integral multiple of the rotary vibration frequency, then the stick–slip vibration will cause strong longitudinal resonance of the wheelset, which indicates large dynamic loads, and wheel tread spalling or potential safety accidents may occur [13].

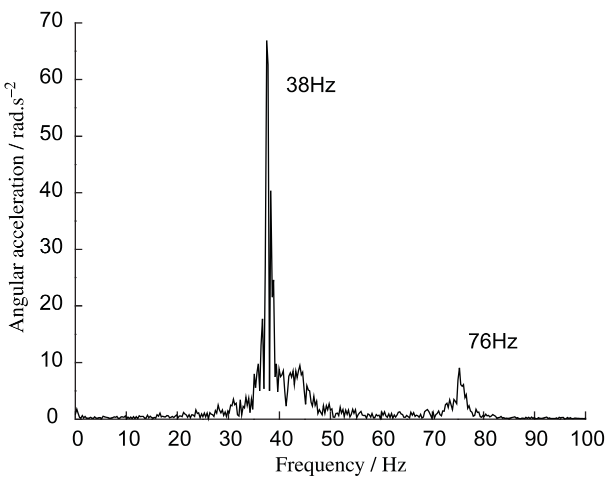

Figure 7. Acceleration frequency spectrum of wheelset rotary vibration.

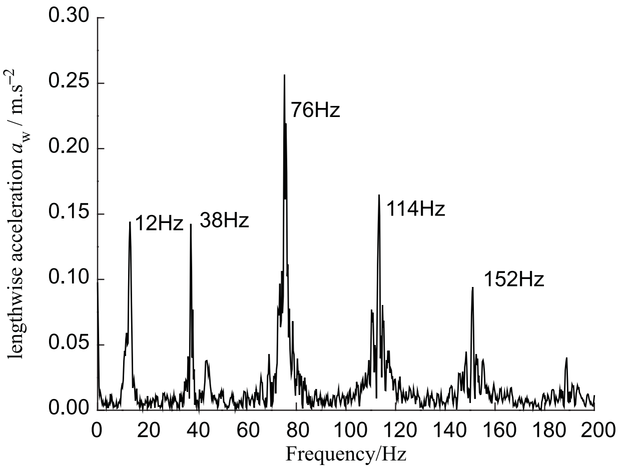

Figure 8. Acceleration frequency spectrum of wheelset longitudinal vibration.

4. The simulation analysis of locomotive stick–slip vibration

4.1. *Train system dynamics model*

A dynamics model of a train system is established with the software SIMPACK. This model is composed of a locomotive and 10 vehicles as shown in Figure 9. The train hauling load is considered, and the unit vehicle is simulated by a mass block which has single degree of freedom along track direction, where the mass blocks are connected by coupler force. The axle load of the locomotive and the vehicle are 23 and 21 tonnes, respectively. The locomotive is equipped with Co′Co′ axle arrangement and the uniaxial power is 1600 kW. The locomotive driving system adopts integral structure, where the gear box is installed on the wheelset and can rotate around it. The motor is suspended under the frame by a rod such as the one shown

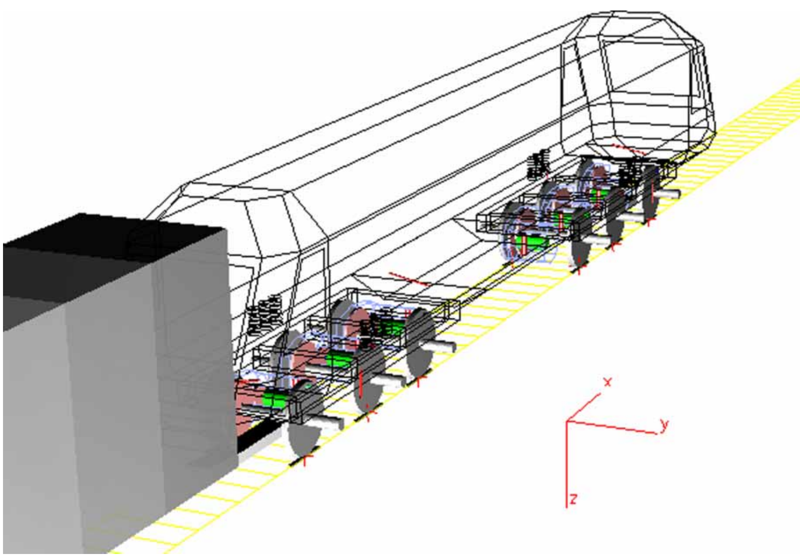

Figure 9. The train system dynamics model.

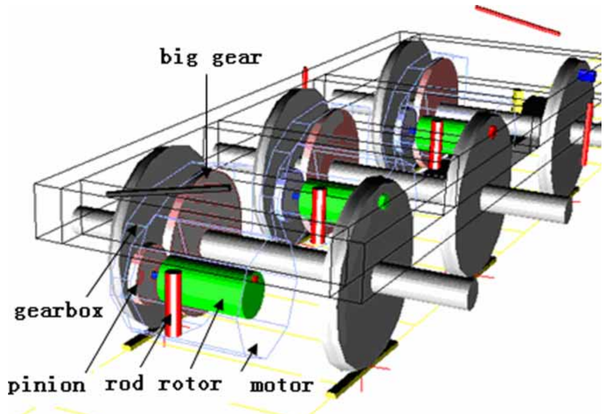

Figure 10. The drive system model.

in Figure 10. This driving system model includes a motor, a gearbox, a rotor, a hang rod, a pinion, a large gear, and their degrees of freedom which are shown in Table 1. The high-power locomotive driving system uses flexible coupling between rotor and pinion, the torsional stiffness of the flexible coupling is 1.36×10^7 Nm/rad.

By taking the train running environment into account, the train resistance is composed of the basic resistance and the additional resistance of the ramp way. The train runs uniformly when the locomotive traction force and resistance are balanced. The unit weight resistance is given below:

$$w = a + b \cdot v + c \cdot v^2 \quad \text{(N/kN)}. \tag{9}$$

In the formula, a, b and c are resistance coefficients, v the train speed and i the slope of ramp way. In this section, the dynamics model adopts the US 5 class track unevenness, JM3 worn-type wheel tread and standard 60 kg/m rail shape.

The dynamics model can simulate actual dynamic processes during the locomotive traction operation. This model can cover more uncertain factors in the locomotive adhesion control than the simple mechanical model with a single wheel.

4.2. *The characteristics of W/R adhesion*

The tangential force coefficient decreases when increasing the W/R slip velocity. This corresponds to the negative slope characteristic of adhesion curves. According to some investigation,

Table 1. The freedoms of locomotive dynamics model.

Element	Lengthwise	Lateral	Vertical	Roll	Pitch	Yaw
Car	X_c	Y_c	Z_c	Φ_c	θ_c	Ψ_c
Frame	X_{fi}	Y_{fi}	Z_{fi}	Φ_{fi}	θ_{fi}	Ψ_{fi}
Motor (gearbox)					θ^a_{bj}	
Hang rod				Φ_{rj}	θ_{rj}	
Rotor					θ_{mj}	
Small gear					θ_{gj}	
Wheelset (big gear)	X_{wj}	Y_{wj}	Z^a_{wj}	Φ^a_{wj}	θ_{wj}	Ψ_{wj}
Vehicle	X_{vk}					

[a]Dependent freedoms: $i = 1$–2, $j = 1$–6 and $k = 1$–10.

the adhesion curves are different under different rail surface conditions. These differences include the maximal tangential force coefficient, the slip rate which corresponds to this maximal tangential force coefficient, the linear slope near the origin and the negative slope at slippage. These can be defined as the four factors of adhesion. The W/R friction coefficient f as a function of the contact patch sliding velocity [14] can be written as follows:

$$f = \frac{f_s}{1 + F\upsilon_c}. \tag{10}$$

In Equation (10), f_s is the static friction coefficient, F the dynamic friction effect coefficient and υ_c is the sliding velocity of the contact patch.

By modifying the W/R tangential force calculation program of Shen *et al.* [15] according to Equation (10), we can obtain the wheel–rail tangential force coefficient curves including the negative slope characteristic, as shown in Figure 11. With the increase of locomotive velocity, the negative slope characteristic becomes obvious. In addition, changing the Kalker weight coefficient K and the dynamic friction influence coefficient F simulates the four factors of the adhesion curves (Figure 12). Therefore, we can obtain the different shapes of tangential force coefficient curves [16,17].

4.3. *The electric driving system of the locomotive*

The high-power locomotives adopt the ‘AC–DC–AC’ traction driving system because of the high-power density and the hardened mechanical characteristics of the AC motor. Presently, the main high-power locomotives use induction motor and vector control. The rotor-flux-oriented vector controller decouples the stator current into two vertical directions: the magnetic field current component and the torque current component through vector transform, and they are controlled respectively [18]. This makes the AC motor have improved speed regulating control similar to that of the DC motor. In order to simplify the electric driving system model and to improve the computing velocity, the AC motor has the same power as the separately excited DC motor. The DC motor also has the same hardness mechanical properties as the AC motor by reducing its rotor resistance [19].

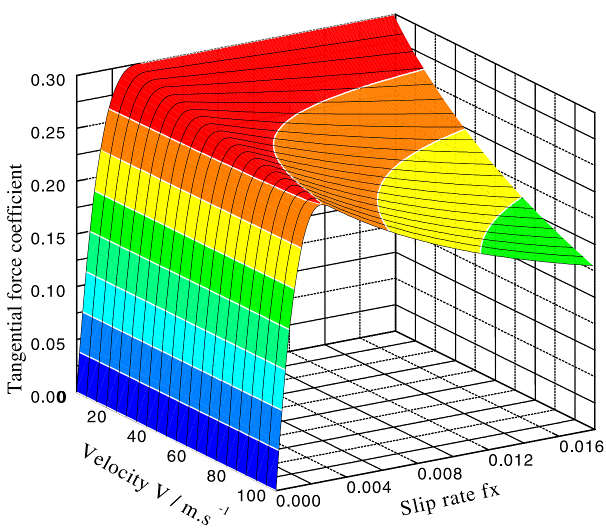

Figure 11. The tangential force coefficient surface.

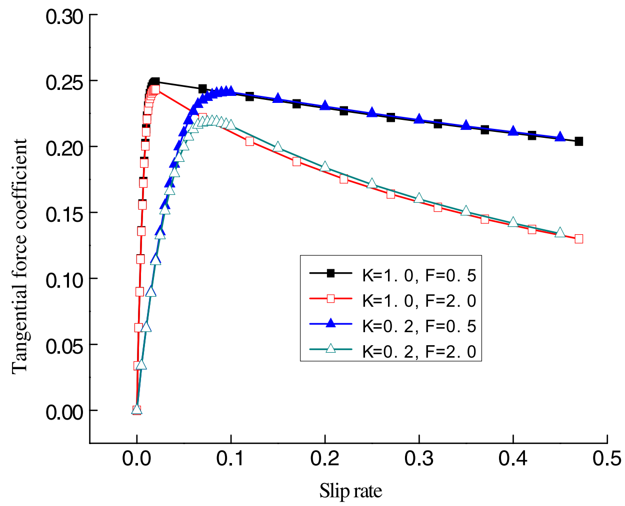

Figure 12. The tangential force curves with different K and F.

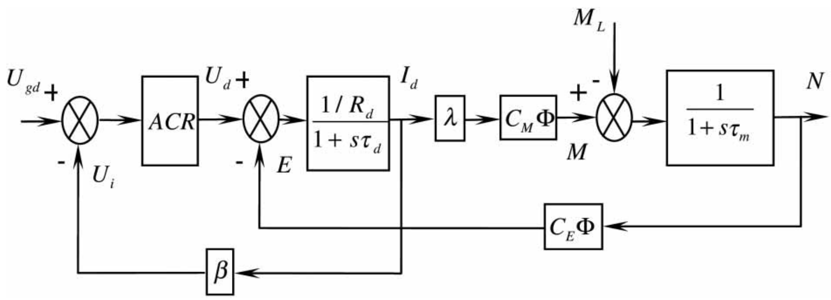

Figure 13. DC motor speed regulating with constant current.

In order to improve the traction performance and simplify the driver manual operation in the locomotive electric driving system, the automatic control should play an important role. The closed-loop-feedback control system includes constant voltage control (i.e. constant speed), constant current control (i.e. constant torque) and current–voltage double closed-loop control. Our study uses a constant-current speed control system. The control block diagram is shown in Figure 13.

In Figure 13, ACR is the PI regulator, C_{E} and C_{M} the motor electromagnetic constant and the torque constant, respectively, Φ the excitation flux, τ_d, τ_m the electromagnetic time constant and the mechanical time constant, respectively, β the current feedback coefficient, λ the axle load transfer coefficient, R_d the rotor resistance and U_{gd} the voltage value.

4.4. *The effects of locomotive parameters on stick–slip vibration*

The dynamics model of a train system applies constant torque on the motor and drives the train, running on a straight line with an initial velocity of 80 km/h. The W/R contact static friction coefficient U_r is shown in different moments in Figure 14. With the decrease of U_r, slippage occurs and the adhesion recovers after 8 s. When U_r decreases and recovers, the wheelset changes into stick–slip vibration state.

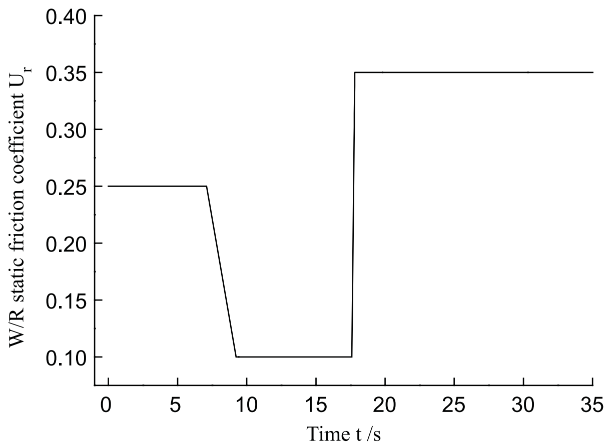

Figure 14. The W/R contact static friction coefficient.

Figures 15–18 show different impacting factors on the stick–slip vibration. It reveals that the longitudinal axle guidance stiffness and the motor suspension stiffness have more significant effects on the stick–slip vibration than the others. It also shows that the shaft-coupling torsional stiffness has lesser influence and the track irregularity has no influence on the stick–slip vibration.

Figure 17 shows the simulation results of the longitudinal slip rates with the original longitudinal axle guidance stiffness K_x and one-tenth of its original value, respectively. The wheelset will go into slip state when U_r decreases. When K_x is getting larger, the wheelset will enter directly into full slip state. Then the W/R adhesion negative damping raises the system vibration energy and enlarges the vibration scope of longitudinal slip rate, and the wheelset will enter into the stick–slip state before U_r increases. Then the wheelset quickly returns to the stick state when U_r starts to increase. For a smaller K_x, the vibration scope of the slip rate is larger and the stick–slip vibration occurs. The wheelset transforms into the full slip state gradually when U_r starts to decrease. When U_r increases, the wide scope of the slip rate prolongs the recovery adhesion time. The simulation results are consistent with the conclusions of the stick–slip vibration stability in Section 3.1.

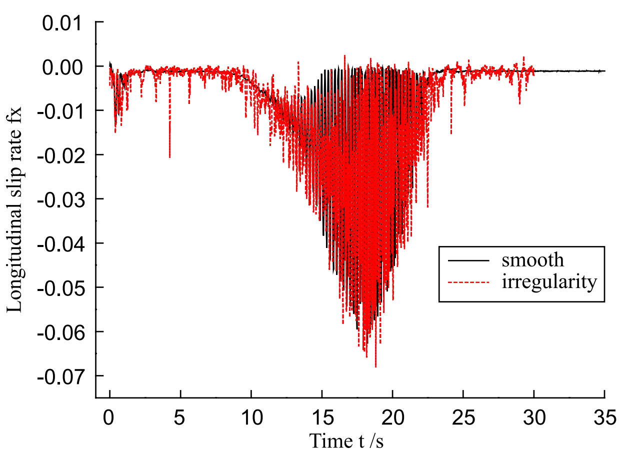

Figure 15. Effect of track irregularity on stick–slip vibration.

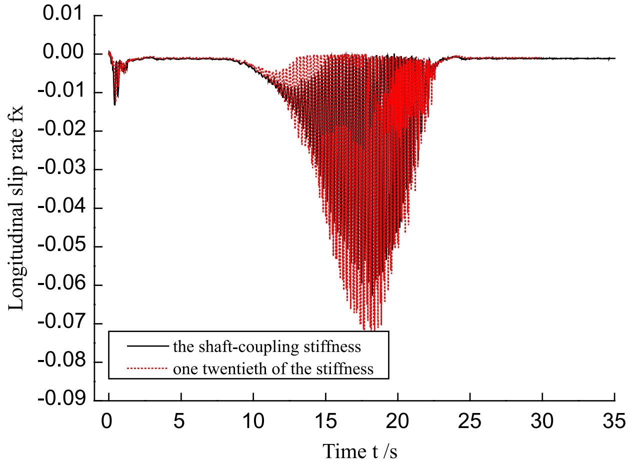

Figure 16. Effect of shaft-coupling torsional stiffness on stick–slip vibration.

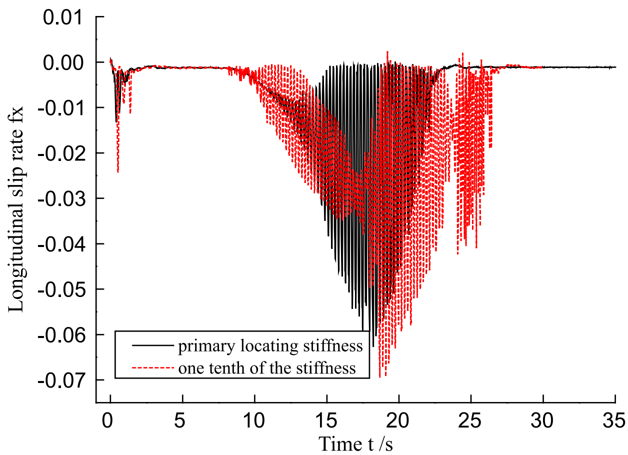

Figure 17. Effect of primary locating stiffness on stick–slip vibration.

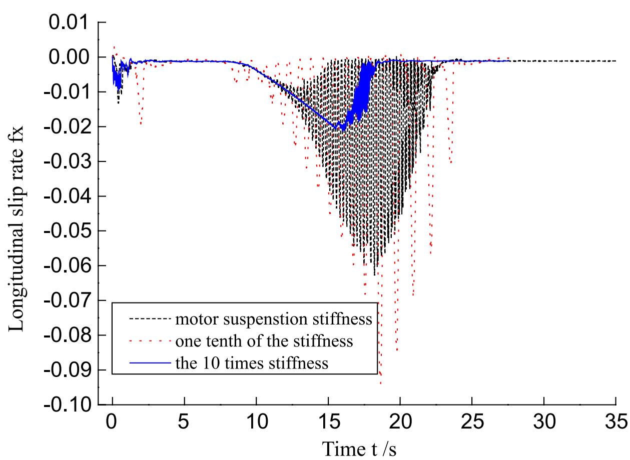

Figure 18. Effect of motor suspension stiffness on stick–slip vibration.

Figure 18 shows the simulation of longitudinal slip rates with respect to different motor suspension stiffness. While the motor suspension stiffness increases, the recovery adhesion time decreases. Figure 18 also indicates that smaller the motor suspension stiffness, larger the wheelset longitudinal slip rate, longer the recovery adhesion time and smaller the locomotive's traction capacity. In addition, the frequency of wheelset longitudinal slip rates depends mainly on the motor suspension stiffness, which confirms the conclusion that the wheelset longitudinal vibration frequency depends on the driving system torsional stiffness as concluded in Section 3.2.

4.5. *Frequency analysis of the stick–slip vibration*

In order to verify the previous theory, we obtain the frequency spectrums of the driving system vibration acceleration during the process of stick–slip vibration. The pitching vibration angular acceleration of the motor and the wheelset longitudinal vibration acceleration are shown in Figures 19 and 20, respectively. In the figures, the motor suspension stiffness is one-tenth of the original design value. The main frequency of the motor pitching vibration is 14 Hz, which is the natural frequency of the pitching vibration. The main frequency of the wheelset longitudinal vibration is 14 Hz and its integer multiple frequencies are obvious when the natural frequency of the wheelset longitudinal vibration is 12 Hz. Different from the conclusions in Section 3.2, the amplitude of double pitching natural frequency is smaller than the value of the foregoing conclusions, because the longitudinal axle guidance damping weakens this high-frequency vibration.

Similarly, the stick–slip vibration can cause the longitudinal vibration of the wheelset, the motor pitching and the wheelset longitudinal vibrations are coupled with the longitudinal tangential force. Likewise, the wheelset's longitudinal vibration causes the longitudinal forced vibration of the frame. Therefore, it needs to rationally match the motor suspension stiffness, the longitudinal axle guidance stiffness and the locomotive drawbar stiffness in order to avoid the strong longitudinal resonances of locomotive structures during the process of stick–slip vibration.

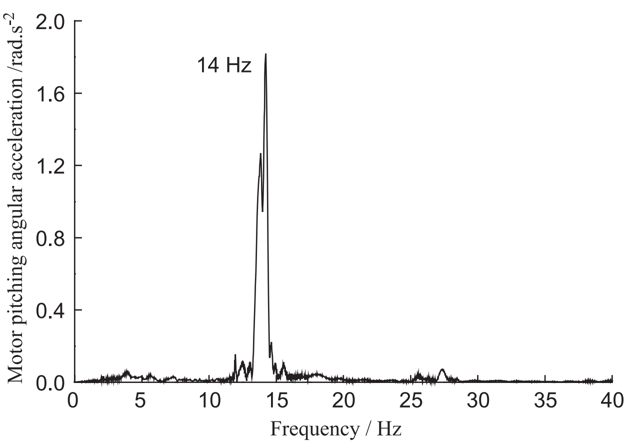

Figure 19. The frequencies of motor pitching.

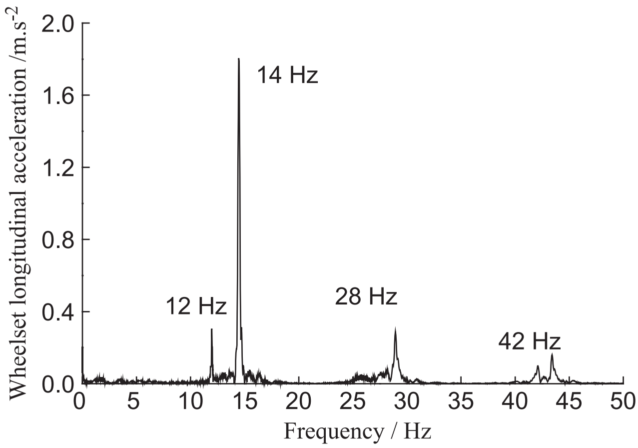

Figure 20. The frequencies of wheelset longitudinal vibration.

5. Parameter matching study on the high-adhesion performance locomotive

5.1. *Locomotive adhesion control*

The adhesion control uses a fuzzy strategy. The fuzzy control does not need an accurate mathematical model and it gives strong self-adaptive and robust performance. Thus, it has good control performances [20] in the different tracks under different adhesion conditions. In this model, the locomotive adhesion control adopts bogie control, that is, the motor torque of each axis in the same bogie will decrease in the same level when slippage is detected. The bogie control has a higher adhesion performance relative to the vehicle control. In this section, we will calculate the difference between the maximum and the minimum of the axles which are located in the same bogie at the same time. Then we perform the real-time calculations for the adhesion level Adl, after filtering. Finally, the control makes re-adhesion by multiplying Adl with the motor torque command [21]. The control system block diagram is shown in Figure 21.

The value of Adl can be obtained by fuzzy reasoning, the rule of which is shown in Figure 22. When the wheelset is in the stick state, the angular velocity and the angular acceleration of the axles in the same bogie are basically identical. Δv and Δa are two small numbers. The

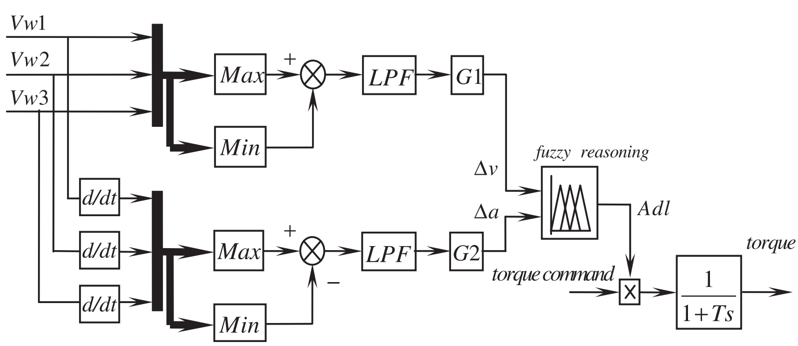

Figure 21. Re-adhesion control block graph of bogie control.

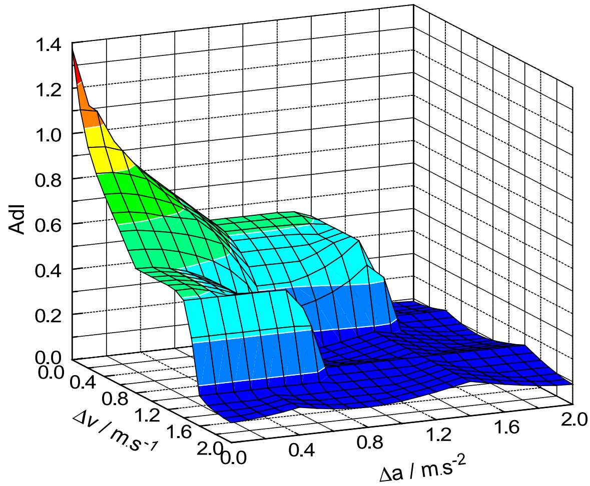

Figure 22. The fuzzy reasoning rules.

corresponding Adl is a large quantity. When the wheelsets are sliding, $\Delta\nu$ and Δa will increase, and the corresponding Adl becomes smaller. The torques of these motors will then decrease, so it will recover to adhesion. Adl can be of a value greater than one, which is in the case of the good track surface conditions. Increasing the torques of these motors will result in a bigger adhesion force. When $\Delta\nu$ and Δa are small, increasing the surface gradient can result in more sensitive adhesion control. With the help of the adhesion control, the longitudinal tangential force of the wheelset can be maintained near the peak of wheel–rail adhesion and so the locomotive has a better traction performance.

The W/R effective adhesion coefficients with the adhesion control under different track surface conditions are shown in Figure 23 (no track irregularity). The adhesion coefficients are distributed around the peak and are strongly affected by the fuzzy control.

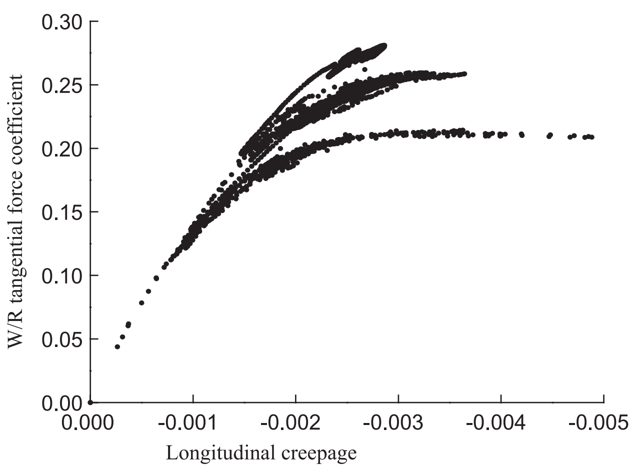

Figure 23. The W/R effective tangential force coefficient with control.

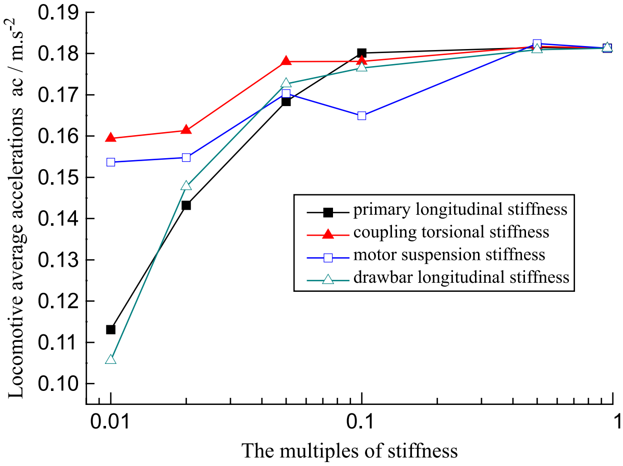

Figure 24. Average accelerations of locomotive with different structure parameters.

5.2. *Parameter matching principles of high-adhesion performance locomotive*

The theoretical results show that the mechanical structure parameters of the locomotive have a great influence on the wheelset stick–slip vibration stability. We can calculate the average acceleration of the train running on a straight line by changing the locomotive's structure parameters. The parameters include the longitudinal axle guidance stiffness, the coupling torsional stiffness, the motor suspension stiffness and the drawbar longitudinal stiffness. In this train system model, the motor adopts constant current control and applies adhesion control. Under the same operating conditions, the traction performance of the locomotive depends on the wheelset adhesion performance.

The results of the calculation are shown in Figure 24. We can see that the adhesion performance is improved when the stiffness increases. The adhesion performance of the locomotive decreases when the motor suspension stiffness is one-tenth of the original value. This is because the stick–slip vibration causes the wheelset's longitudinal resonance.

We are able to reach a conclusion on the parameter matching principle. To obtain a high-adhesion performance of the locomotive and avoid intensive longitudinal resonance of the wheelset when the stick–slip vibration occurs, it is beneficial to increase the locomotive structure parameters indicated previously and optimise the matching of the motor suspension stiffness with the longitudinal axle guidance stiffness.

6. Conclusions

(1) The stick–slip vibration is a dynamic process alternating between stick state and slip state. The stability of this process depends on the positive and negative damping of the wheelset adhesion. We performed theoretical analysis on the stick–slip vibration according to the mean and the dynamic slip rate. It shows that decreasing the mean slip rate and the dynamic slip rate will improve the stability of the stick–slip vibration.

(2) When the stick–slip vibration occurs, the rotary and the longitudinal vibrations of the wheelset are coupled with the longitudinal tangential force. The longitudinal vibration frequencies of the wheelset are integral multiples of the natural frequency of the driving system. The largest energy occurs at the frequency twice the natural frequency.

(3) A train system dynamics model integrated with electromechanical and control system is established to simulate the stick–slip vibration phenomenon under saturated adhesion to verify the theoretical analysis. The simulation result shows that increasing the longitudinal axle guidance stiffness, the motor suspension stiffness and the drawbar longitudinal stiffness is beneficial to improve the locomotive adhesion performance and the stability of the stick–slip vibration.
(4) When the stick–slip vibration occurs, the main frequencies of the wheelset longitudinal vibration are equal to the motor pitching frequency and its integral multiples. Therefore, it requires optimisation of the matching of the motor suspension stiffness and the longitudinal axle guidance stiffness to avoid the longitudinal resonance of the structure.

Acknowledgement

The authors wish to acknowledge the support of the National Natural Science Foundation of China (No. 50875219).

References

[1] T. Hirotsu, S. Kasai, and H. Takai, *Self-excited vibration during slippage of parallel cardan drives for electric railcars*, JSME Int. J. 30 (1987), pp. 1304–1310.
[2] Y.F. Wu, *Stability analysis of the vibration of the frame-mounted motor driving system*, J. China Railw. Soc. 14 (1992), pp. 1–7.
[3] S. Muller and R. Kogel, *Numerical simulation of roll-slip oscillations in locomotive drives*, Z. Angew. Math. Mech. 81 (Suppl.) (2001), pp. 61–64.
[4] X. Sun, *The locomotive system design of high adhesion performance*, J. Southwest Jiaotong Univ. 29 (1994), pp. 235–247.
[5] B. Koansok, K. Keiji, and N. Tsunamitsu, *An experimental investigation of transient traction characteristics in rolling–sliding wheel/rail contacts under dry–wet conditions*, Wear 263 (2007), pp. 169–179.
[6] W.H. Zhang, J.Z. Chen, and X.J. Wu, *Wheel/rail adhesion and analysis by using full scale roller rig*, Wear 253 (2002), pp. 82–88.
[7] O. Polach, *Influence of locomotive tractive effort on the forces between wheel and rail*, Veh. Syst. Dyn. 35 (Suppl.) (2001), pp. 7–22.
[8] O. Polach, *A fast wheel-rail force calculation computer code*, Veh. Syst. Dyn. 33 (Suppl.) (1999), pp. 728–739.
[9] S.Y. Ren, J.H Bao, and J.W. Zhang, *Modeling and simulation of the self-excited torsional vibration of driveline for SZG 4031 towing tractor under heavy load*, J. Vib. Shock 24 (2005), pp. 95–101.
[10] F.T. Wang, *Vehicle System Dynamics*, Shanghai Railway University Press, Shanghai, 2004.
[11] M. Ertz and K. Knothe, *Thermal stresses and shakedown in wheel/rail contact*, Arch. Appl. Mech. 72 (2003), pp. 1521–1533.
[12] Y. Yao, H.J. Zhang, and Y. Luo, *Longitudinal vibration analysis of wheelset on locomotive under slippage*, Chin. J. Mech. Eng. 45 (2009), pp. 199–203.
[13] S.H. Luo, D.C. Jin, and Q. Chen, *Study on longitudinal vibration of wheelsets and related problems of rail vehicles*, J. China Railw. Soc. 27 (2005), pp. 26–34.
[14] X.S. Jin and L.M. Zhang, *Numerical analysis of the driving torque applied to a single wheelset of locomotive with high speed*, Chin. J. Mech. Eng. 35 (1999), pp. 56–60.
[15] Z.Y. Shen, J.K. Hedrick, and J.A. Elkins, *A Comparison of Alternative Creep-force Models for Rail Vehicle Dynamic Analysis*. Proceedings of the 8th IAVSD Symposium, Cambridge, MA, Swets and Zeitlinger, Lisse, 1984, pp. 591–605.
[16] Y. Yao, H.J. Zhang, and Y. Luo, *Torsional-longitudinal coupling vibration analysis of drive system on locomotive*, J. Traffic Transp. Eng. 9 (2009), pp. 13–17.
[17] Y. Yao, H.J. Zhang, and K. Chen, *Self-excited torsional vibrations of drive system on locomotive under slippage*, J. Southwest Jiaotong Univ. 43 (2008), pp. 762–766.
[18] T.X. Mei, J.H. Yu, and D.A. Wilson, *Wheelset Dynamics and Wheel Slip Detection*, Proceedings of 2006 International Symposium on Speed-up and Service technology for Railway and Maglev System, STECH'06 Southwest Jiaotong University Press, Chengdu, Sichuan, P. R. China, 2006, pp. 40–46.
[19] S. Leva, A.P. Morando, and P. Colombaioni, *Dynamic analysis of a high-speed train*, Veh. Technol. 57 (2008), pp. 107–119.
[20] K. Sun, H. Uk, and K. Hak, *Re-adhesion control with estimated adhesion force coefficient for wheeled robot using fuzzy logic*, IEEE/IECON'2004, Pusan, 2004.
[21] L.M. Song, *The Transmission System and Control of EMU*, China Railway Press, Beijing, 2007.